 

# Contribution of continental subduction to very light B isotope signatures in post-collisional magmas: evidence from southern Tibetan ultrapotassic rocks

Lu-Lu Hao[a, b], Qiang Wang[a, b, c*], Andrew C. Kerr[d], Gang-Jian Wei[a, b], Fang Huang[e, f], Miao-Yan Zhang[a, c], Yue Qi[a, b], Lin Ma[a, b], Xue-Fei Chen[a, b], Ya-Nan Yang[a, b]

[a] State Key Laboratory of Isotope Geochemistry, Guangzhou Institute of Geochemistry, Chinese Academy of Sciences, Guangzhou 510640, China

[b] CAS Center for Excellence in Deep Earth Science, Guangzhou, 510640, China

[c] College of Earth and Planetary Sciences, University of Chinese Academy of Sciences, Beijing 100049, China

[d] School of Earth and Environmental Sciences, Cardiff University, Cardiff, CF10 3AT, UK

[e] CAS Key Laboratory of Crust-Mantle Materials and Environments, School of Earth and Space Sciences, University of Science and Technology of China, Hefei 230026, China

[f] CAS Center for Excellence in Comparative Planetology, University of Science and Technology of China, Hefei, Anhui 230026, China

*Corresponding author:*
***Qiang Wang,*** *State Key Laboratory of Isotope Geochemistry, Guangzhou Institute of Geochemistry, Chinese Academy of Sciences, Guangzhou, 510640*
*E-mail: wqiang@gig.ac.cn*

## Abstract

Understanding the subduction and recycling of continental crust is crucial for reconstructing the long-term evolutionary history of Earth's mantle and crust. The Himalaya-Tibet orogen is arguably the world's best natural laboratory for investigating these processes. Cenozoic post-collisional ultrapotassic volcanic rocks are common in the Lhasa block of southern Tibet and they can provide important clues to crust-mantle interaction in a well-characterized continental collision zone. Understanding the sources and processes that generated these lavas can contribute to our understanding of the thermal and compositional characteristics of the deep mantle and geodynamic processes in this region, including Indian continental subduction. In this contribution, we report Sr-Nd-Pb-O-B isotope and elemental chemistry data for post-collisional (13-11 Ma) ultrapotassic rocks from the TangraYumco-Xuruco rift (TYXR) in the Lhasa block. The arc-like trace-element signatures and markedly enriched Sr-Nd-Pb-O isotope compositions indicate that these mafic rocks originate from a mantle source containing recycled crustal components. Unlike pre-collisional (~64 Ma) ultrapotassic rocks in the Lhasa block with arc-like B/Nb (0.85-1.89) and $\delta^{11}B$ (-9.0 to -2.5‰) values, the TYXR post-collisional ultrapotassic rocks with much lower B/Nb (0.05-0.85) and $\delta^{11}B$ (down to -20.5‰) values resemble Miocene K-rich volcanic rocks from western Anatolia. These western Anatolian rocks have been formed by either progressive dehydration of a stalled slab or deep-subducted continental crust. However, some TYXR samples have lower B/Nb ratios than MORB, consistent with a fluid-starved source. These markedly negative $\delta^{11}B$ in conjunction with low B/Nb cannot be explained by the addition of melts from oceanic sediments, which generally yield lower B/Nb but higher $\delta^{11}B$ values than MORB (e.g., the Armenia post-collisional mafic rocks). Given the low $\delta^{11}B$ of Indian upper continental crust and its similar Sr-Nd-Pb isotopic signatures to the post-collisional lavas, it is clear that the post-collisional ultrapotassic rocks in the Lhasa block contain a significant component derived from subducted Indian continental crust. Combined with the temporal evolution of regional magmatism, tectonics and geophysical data, we propose that the break-off and tearing of subducted Indian continental slab induced post-collisional magmatism in the Lhasa block. Our case study provides evidence that continental subduction contributes to very light B isotope compositions of post-collisional magmas, which suggests that B isotopes have the potential to discriminate between oceanic subduction and continental subduction.

**Key words:** Boron isotopes, continental subduction, mantle metasomatism, post-collisional ultrapotassic magmatism, Tibetan Plateau

# 1. Introduction

Subduction zones are the primary sites for mass and energy exchange between the mantle and the crust (e.g., Stern, 2002; Elliott, 2004). Recycling of crustal materials into the mantle by subduction is arguably the most important mechanism that creates geochemical and lithological heterogeneities in the mantle. Recycling of sedimentary material in oceanic subduction zones have been widely studied and convincing evidence exists on the long-term effects of sediment recycling in mantle evolution (e.g., Willbold and Stracke, 2010). However, recycling of continental crust material to the deep mantle is more controversial. Recent studies suggest that subduction erosion of the overlying crust plays an important role in arc magmatism (e.g., Vennucci et al., 2004; Gomez-Tuena et al.,2018). In comparison, subduction of continental crust is much less studied and thus understood. However, during much of Earth's history, continental subduction may have also been important (see a review of Ducea, 2016).

The Himalaya-Tibet plateau is one of the best places on earth to study continental subduction and the fate of subducted continental crust material in the mantle. The most difficult aspect of studying the interactions between subducted continental crust and the mantle is the availability of related magmas, and our ability to distinguish between many similar components involved in their petrogenesis, including upper crust vs. subducted crust vs. subducted sediments; subcontinental mantle vs. metasomatized mantle wedge vs. stalled oceanic crust. In this study we attempt to fill some of these gaps by combining B isotopes with more traditional geochemical data.

Partial melting of mantle sources metasomatized by oceanic subduction yields a variety of mafic igneous rocks at convergent plate boundaries (e.g., Elliott, 2004). These metasomatized mantle sources do not always immediately melt after their formation but can be stored at sub-solidus temperatures in the mantle wedge for variable timescales, ranging from few to hundreds of million years (e.g., Zheng and Chen, 2016). Subsequent asthenosphere upwelling can melt or remobilize these metasomatized sources to generate mafic magmatism in still active continental margins or post-subduction settings. An increasing number of studies have reported post-collisional mafic rocks with mantle sources that are closely related to preceding oceanic subduction (e.g., Azizi et al., 2021). Continental subduction can also cause crust-mantle interaction in the subduction channel (Conticelli et al., 2009; Soder and Romer, 2018). Felsic melts derived from deep-subducted continental crust interact with the subcontinental lithospheric mantle wedge peridotite to produce fertile mantle sources (e.g., Dai et al., 2015). No syn-subduction arc-type magmatism has, thus far, been found above continental subduction zones, likely due to limited aqueous fluids in the subducted continental crust and/or their low temperature (Zheng and Chen, 2016). However, mafic magmatism has been found in continental collision zones with post-collisional ages, that is most likely due to orogenic lithospheric extension. Given that continental subduction is generally induced by gravitational traction of the oceanic lithosphere, both oceanic and continental crustal materials can be recycled into the mantle in continental subduction zones and contribute to post-collisional mafic magmatism (Dai et al., 2015). Identifying recycled crustal components in continental collisional orogens is therefore important in our efforts to understand the development from oceanic to continental subduction and the evolution of orogenic belts.

Cenozoic post-collisional mafic igneous rocks are common in the Himalaya-Tibet orogen (e.g., Chung et al., 2005; Yakovlev et al., 2019). Numerous studies have focused on these mafic rocks because they provide a unique post-collisional window into the thermal and compositional characteristics of the deep mantle and the dynamic processes that resulted in the uplift of the Tibetan Plateau (Williams et al., 2001; Guo and Wilson, 2019). The post-collisional mafic ultrapotassic rocks in the Lhasa block of southern Tibet are generally considered to be products of Indian continental subduction. However, different views exist regarding whether their mantle source was metasomatized by subducted Indian continental crust (e.g., Ding et al., 2003; Mahéo et al., 2009; Hao et al., 2018) or Neo-Tethys oceanic sediments (e.g., Gao et al., 2007, Liu et al., 2015). Understanding the nature of this metasomatism is crucial in understanding mantle dynamics in this region, including earthquake predictions. Recently, recycled continental crust has been identified using stable isotopes (e.g., Mg, Ca, Li) in post-collisional mafic magmas in southern Tibet. The light Mg and Ca isotope signatures of these post-collisional rocks point to recycled carbonate components in their mantle source (e.g., Liu et al., 2015).

However, carbonates are also found on the Indian continental platform and Mg-Ca isotopes cannot distinguish between an oceanic or continental origin (Guo and Wilson, 2019). Based on low $\delta^7$Li values (down to -3.9‰) of the ultrapotassic rocks in the Lhasa block, Tian et al. (2020) argued that these rocks originated from Indian continental crust rather than an oceanic plate. This is because most modern arcs have $\delta^7$Li comparable to, or higher than, those of MORB ($\delta^7$Li= +3.5± 1.0‰, Marschall et al., 2017). However, some arcs (e.g., Lesser Antilles, Tang et al., 2014) have low $\delta^7$Li (down to -1.0‰). Furthermore, Agostini et al. (2008) reported very low $\delta^7$Li (down to -4.0‰) for calc-alkaline arc rocks from western Anatolia. Thus, the origin of light Li isotope compositions of post-collisional rocks in the Lhasa block remains unclear.

Boron isotope and concentrations have the potential to discriminate between oceanic subduction and continental subduction (e.g., Palmer et al., 2019; De Hoog and Savov, 2017). Due to interaction with seawater which has highly positive $\delta^{11}$B (+39.6‰, e.g., Foster et al., 2010), subducted oceanic slabs have overall positive B isotope ratios, including altered oceanic crust ($\delta^{11}$B = 0~ +18‰) and marine sediments ($\delta^{11}$B = +2~ +26‰). The serpentinized fore-arc mantle wedge ($\delta^{11}$B = +5~ +25‰) and eroded lower crustal material may also be important sources of B (e.g., Tonarini et al., 2011). Modern arc lavas generally have higher B concentrations, B/Nb ratios, and $\delta^{11}$B values than the depleted mantle and MORB ($\delta^{11}$B = -7.1± 0.9‰, Marschall et al., 2017), which is generally ascribed to contribution of B-rich fluids with a heavy B isotope signature liberated from subducted oceanic slabs. However, continental crust mainly consists of crystalline basement and continental sediments which typically have low $\delta^{11}$B (-9.1± 2.4‰, Trumbull and Slack, 2018). Fluids/melts released from subducted continental crust should have much lighter B isotope compositions than oceanic slab-derived melts and fluids, unless the slab is extremely dehydrated. Palmer et al. (2019) ascribed the low $\delta^{11}$B values (down to -31~ -20‰) of Miocene K-rich rocks in western Anatolia to contribution from subducted continental crust. However, other studies have suggested that these low $\delta^{11}$B values could be derived from a stalled and extremely dehydrated oceanic slab (Tonarini et al., 2005; Agostini et al., 2008; Sugden et al., 2020).

Southern Tibet is an excellent place to test these competing ideas as there is no question, based on seismic evidence, that continental crust was subducted in this region (e.g., Replumaz et al., 2010). Combining B isotopes with traditional Sr-Nd-Pb-O isotopes can help differentiate the continent vs. oceanic origin of low $\delta^{11}B$ signatures. In this paper therefore, we report B concentrations and $\delta^{11}B$ data for post-collisional (13-11 Ma) ultrapotassic rocks, as well as pre-collisional (~64 Ma) ultrapotassic rocks from the Lhasa block in southern Tibet with the latter being derived from a primarily oceanic slab-modified mantle. Combined with elemental and Sr-Nd-Pb-O isotope data, we are able to determine the nature of recycled crustal components in post-collisional mantle. Our results indicate that the very light B isotope compositions of these post-collisional ultrapotassic rocks originated from recycled Indian continental crust. This is the first time that B isotope systematics have been used to explore the post-collisional mantle in southern Tibet and trace Indian continental subduction.

## 2. Geological background and sample characteristics

The Himalaya-Tibet orogen consists of the Himalaya, Lhasa, Qiangtang, and Songpan-Ganze blocks from south to north, and these are separated from each other by the Indus-Yarlung-Zangbu (IYZ), Bangong-Nujiang (BN), and Jinsha (JS) sutures, respectively (Yin and Harrison, 2000). The Lhasa block in southern Tibet was the last terrane to be accreted onto Eurasia in the late Mesozoic before the collision with the northward-drifting Indian plate during the early Cenozoic (e.g., Zhu et al., 2011). The IYZ suture between the Lhasa and Himalaya blocks represents the remnant of the Neo-Tethys Ocean. The Neo-Tethys oceanic slab was subducted northwards beneath the Lhasa block from the Triassic to late Cretaceous. In the early Cenozoic (~60-55 Ma), the initial India-Eurasia (Himalaya-Lhasa) collision occurred (e.g., Hu et al., 2015). During the syn-collisional stage, Indian continental plate was dragged downwards by subducted Neo-Tethys oceanic slab. The buoyancy of the continental plate counteracted the oceanic slab pull and eventually resulted in break-off of the oceanic slab at ~45 Ma (e.g., Mahéo et al., 2009) and cessation of oceanic subduction. After oceanic slab break-off, between 25 and 8 Ma, post-collisional magmatism comprising adakitic granitoids and potassic-ultrapotassic lavas was common in the Lhasa block (Guo and Wilson, 2019) (Fig. 1A).

The Miocene post-collisional ultrapotassic lavas investigated in this study were collected from four volcanic fields (Yaqian, Mibale, Daguo, and Chazi from north to south) located within the north-south-trending TangraYumco-Xuruco rift (TYXR) (Fig. 1B). These rocks typically show porphyritic textures with abundant phenocrysts (up to 1-4 mm in diameter) of clinopyroxene, phlogopite, and K-feldspar with minor olivine (Fig. 2). The fine-grained trachytic groundmass is composed of K-feldspar, biotite, opaque minerals, and glass. Previous studies have determined ages of ~13 Ma, ~12.5 Ma, and ~13 Ma for the Yaqian, Mibale and Daguo K-rich volcanic rocks, respectively (Guo et al., 2013 and references therein). The age of the Chazi K-rich rocks remains uncertain. Ar-Ar dating of phlogopite and sanidine indicates suggests that they erupted at 13-8 Ma (Ding et al., 2003), whereas zircon U-Pb dating yielded more precise ages of ~11.7-11.0 Ma (e.g., Guo et al., 2013; Tian et al., 2017).

We also present B contents and $\delta^{11}B$ data for pre-collisional (~64 Ma) ultrapotassic rocks in Rongniduo of the Lhasa block (Fig. 1A). Detailed sample descriptions, major and trace elemental, and Sr-Nd isotopic data for these rocks are available in Qi et al. (2018). The formation of these older rocks slightly precedes the Himalaya-Lhasa collision, which means that they should be derived from an oceanic subduction-modified mantle, or at the very least, they should have a minimum contribution from continental crust.

## 3. Methods and results

All analyses including whole-rock major- and trace-element and Sr-Nd-Pb-B isotope analyses, and SIMS zircon U-Pb age and O isotope analyses were carried out at State Key Laboratory of Isotope Geochemistry, Guangzhou Institute of Geochemistry, Chinese Academy of Sciences (GIGCAS), Guangzhou, China. A more detailed discussion of the methodology and analytical results are presented in the Appendix.

### 3.1 SIMS zircon U-Pb ages and O isotopes

SIMS zircon U-Pb dating was carried out on four ultrapotassic lava samples from Chazi near the Xuruco (Fig. 3A, S1). These zircon grains are subhedral to euhedral and

CL imaging shows obvious oscillatory or planar zoning, indicating their magmatic origin (Fig. S1). Zircons from sample CZ02-4 yield consistent lower intercept and weighted mean $^{206}Pb/^{238}U$ ages of 11.05± 0.17 and 11.02± 0.29 Ma, respectively. Sample CZ07-1 shows consistent lower intercept and weighted mean $^{206}Pb/^{238}U$ ages of 11.65± 0.23 and 11.64± 0.23 Ma, respectively. Nine analyses of zircons from sample CZ08-1 give similarly consistent lower intercept and weighted mean $^{206}Pb/^{238}U$ ages of 11.17± 0.12 and 11.15± 0.12 Ma, respectively. Finally, a total of 13 analyses of zircon grains from sample CZ12-1 yield lower intercept and weighted mean $^{206}Pb/^{238}U$ ages of 11.26± 0.10 and 11.25± 0.13 Ma, respectively. In summary, SIMS zircon U-Pb dating of the Chazi ultrapotassic rocks produces relatively consistent ages between 11.02± 0.29 and 11.64± 0.23 Ma (Fig. 3A), indicating these rocks erupted in the middle Miocene.

Oxygen isotopes were analyzed on zircon grains in the same domains where U-Pb ages were measured. Twenty-four analyses from three Chazi ultrapotassic rock samples (CZ02-4, 07-1, 08-1) yield a relatively large range of O isotope compositions (Fig. 3B). Twenty-one zircon grains yield high $\delta^{18}O$ values of 6.62-8.99‰ with an average value of 8.12‰, which is similar to published $\delta^{18}O$ data for Chazi ultrapotassic rocks (6.8-8.5‰, Tian et al., 2017). Three zircon grains have low $\delta^{18}O$ values ranging from 4.91± 0.16‰ to 5.26± 0.28‰, with an average value of 5.10‰, which is within the range of normal mantle zircon (5.3± 0.3‰).

## 3.2 Whole-rock major and trace elements

The 39 studied volcanic rocks from the TYXR have intermediate $SiO_2$ contents of 53.1-63.5 wt.% (volatile-free), and high total alkaline contents of 7.6-12.6 wt.%, and thus plot in the fields of basaltic trachyandesite, trachyandesite, and trachyte on the TAS diagram (Fig. 4A). They have high $K_2O$ contents (5.6-10.9 wt.%), $K_2O/Na_2O$ ratios (>2) (Fig. 4B), and MgO (>3 wt.%) contents, and are therefore ultrapotassic rocks. They also have relatively high Cr and Ni contents (up to 430 and 199 ppm, respectively). On the chondrite-normalized REE (rare earth element) diagram (Fig. 5A), all studied ultrapotassic rocks show enriched light REE (LREE) and depleted heavy REE (HREE) patterns with small negative Eu anomalies. However, there are slight differences between the ultrapotassic rocks from each volcanic field. For example, the samples from Chazi, Daguo, and Mibale have flat LREE patterns with $(La/Sm)_N$ = 1.8-3.3, while the Yaqian samples have elevated $(La/Sm)_N$ (4.9-6.2; Fig. 5A). These two types of chondrite-normalized REE patterns have also been reported in post-collisional potassic-ultrapotassic rocks from the Variscan Orogen (Solder and Romer, 2018) and the western Mediterranean region (Conticelli et al., 2009). Primitive mantle-normalized trace-element patterns of all studied ultrapotassic rocks (Fig. 5B) are characterized by marked enrichment in large ion lithophile elements (LILEs, e.g., Rb, Ba, Th), positive Pb anomalies, and negative anomalies of high field strength elements (HFSEs, e.g., Nb and Ta).

## 3.3 Sr-Nd-Pb isotopic compositions

The ultrapotassic rocks from the TYXR show very enriched Sr-Nd isotope compositions with high $^{87}Sr/^{86}Sr(i)$ (0.7163-0.7358), and low $^{143}Nd/^{144}Nd(i)$ (0.5119-0.5120) and εNd(t) (-14.89 to -13.00), similar to other post-collisional ultrapotassic rocks elsewhere in the Lhasa block (Fig. 6). The ultrapotassic rocks from Yaqian, Mibale, and Daguo have relatively homogeneous Sr-Nd isotope compositions, whereas the Chazi rocks show a relatively narrow range in Nd isotopes but a broad range in Sr isotopes. The ultrapotassic rocks from the TYXR (Yaqian, Daguo and Chazi) also show highly radiogenic Pb isotope compositions with $^{206}Pb/^{204}Pb$ = 18.45-19.36, $^{207}Pb/^{204}Pb$ = 15.73-15.79, and $^{208}Pb/^{204}Pb$ = 39.37-40.14 (Fig. 7). These high Pb isotope ratios are similar to those of post-collisional ultrapotassic rocks elsewhere in the Lhasa block. Compared to the limited variations of Pb isotopes of the Yaqian and Daguo ultrapotassic rocks, the Chazi samples have a wider range of Pb isotopes with $^{206}Pb/^{204}Pb$ = 18.83-19.36, $^{207}Pb/^{204}Pb$ = 15.77-15.79, and $^{208}Pb/^{204}Pb$ = 39.77-40.14. In terms of Pb isotope systematics (Fig. 7), all the studied samples fall in the range of typical crustal rocks (Soder and Romer, 2018).

## 3.4 Bulk-rock B concentrations and B isotope compositions

The post-collisional (~13-11 Ma) ultrapotassic rocks from the TYXR have B concentrations of 2.6-30.1 ug/g (ppm) and $\delta^{11}B$ values of -20.5 to -10.3‰. Generally, from south to north, the ultrapotassic rocks show decreasing B contents and $\delta^{11}B$ values (Fig. 8A-B): Chazi (14.3-30.1 ppm, -12.4~ -10.8‰), Daguo and Mibale (7.3-9.4 ppm, -17.0~ -

10.3‰), Yaqian (2.6-7.1 ppm, -20.5~ -12.1‰). All these B isotope compositions are significantly lighter than those of MORB and modern arcs (De Hoog and Savov, 2017; Marschall et al., 2017), including lavas from hot arcs (e.g., Cascades, Leeman et al., 2004) (Fig. 8C). These light B isotope compositions are most similar to those of Miocene ultrapotassic rocks in western Anatolia (-15.0~ -11.2‰) (Tonarini et al., 2005; Agostini et al., 2008) (Fig. 8A, C). Palmer et al. (2019) also reported very low $\delta^{11}B$ values (down to -30~ -20‰) of these western Anatolia Miocene K-rich rocks. The B/Nb ratios of the TYXR ultrapotassic rocks vary from 0.05 to 0.85, which are lower than those of modern arcs (not including hot arcs) but overlap with those of MORB (0.15-1.05, Marschall et al., 2017) and western Anatolia Miocene K-rich rocks (0.28-1.02) (Fig. 8C). The Yaqian ultrapotassic rocks show even lower B/Nb ratios (i.e., 0.05-0.13) than MORB, which have been observed in hot arcs and Armenia post-collisional mafic rocks (Sugden et al., 2020) (Fig. 8C), both of these have been shown to represent melting of fluid-starved sources.

In contrast, the pre-collisional (~64 Ma) ultrapotassic rocks in Rongniduo have higher B/Nb ratios (0.85-1.89) and $\delta^{11}B$ values (-9.0~ -2.5‰) than post-collisional (13-11 Ma) ultrapotassic rocks of the TYXR (Fig. 8) and indicate the close arc affinity. These Rongniduo data are very similar to Oligocene-Miocene calc-alkaline rocks in western Anatolia (Fig. 8A, C) (Tonarini et al., 2005).

# 4. Discussion

## 4.1 Effects of post-eruption alteration, crustal assimilation, and fractional crystallization

Post-collisional ultrapotassic rocks from the TYXR show well-preserved primary minerals (olivine, clinopyroxene, phlogopite, and K-feldspar) with slight alteration and very low loss on ignition (LOI) values (< 2.0 wt.%), suggesting that sub-solidus alteration did not significantly influence their original magmatic compositions. This is consistent with the observation that their B-Sr contents and isotope compositions do not correlate with their LOI values (Fig. S2). Conversely, the ~64 Ma ultrapotassic rocks from Rongniduo have higher LOI values (3.5-5.0 wt.%), possibly indicating significant low-temperature alteration.

However, their Sr isotope ratios remain nearly constant with variable LOI values (Fig. S2d), suggesting that their isotope compositions were not affected by low-temperature process. Their B contents decrease with increasing LOI (Fig. S2a), likely indicating some B has been lost due to alteration. However, the Rongniduo samples still have high B/Nb ratios (Fig. 8C), which are well within those of modern arcs. Furthermore, their restricted B isotope ratios do not correlate with LOI (Fig. S2b), suggesting these data have not been modified significantly by alteration and so are likely to represent mantle source compositions.

It is also important to consider the possible effects of shallow-level processes such as crustal contamination and fractional crystallization. Post-collisional ultrapotassic rocks from Yaqian, Mibale, and Daguo have relatively limited ranges in Sr-Nd isotopic ratios, which do not correlate with $SiO_2$ contents or Mg# values (Fig. S3a-d). Ultrapotassic rocks from Chazi have a wider range of Sr-Nd isotopic ratios that do correlate with $SiO_2$ and Mg#, however, samples with more mafic compositions having more crustal-like Sr-Nd isotopes. This is the converse of what would be expected from crustal assimilation. Furthermore, the Chazi samples have a relatively narrow range of B isotope compositions over a range from 56 to 68 Mg# (Fig. S3e-f), indicating insignificant crustal assimilation. Conversely, their Sr-Nd isotope compositions do correlate with $K_2O$ contents and $K_2O/Na_2O$ ratios (Fig. S3i-j), likely indicating a metasomatized mantle source. The Rongniduo ultrapotassic rocks are essentially uncontaminated with continental crust (Qi et al., 2018).

MgO contents of the TYXR ultrapotassic rocks positively correlate with Ni, Cr, and CaO contents, indicating probable fractional crystallization of olivine and clinopyroxene during magma ascent. Conversely, significant garnet and amphibole fractionation can be excluded because fractionation of these minerals will increase La/Yb ratios (Davidson et al., 2007) and this is not observed in the TYXR ultrapotassic rocks (Fig. 9A). The steep positive correlations of these rocks on La/Yb and La/Sm vs La diagrams (Fig. 9B-C) are consistent with varying extents of partial melting rather than fractional crystallization. Furthermore, post-collisional basaltic or basaltic ultrapotassic rocks are rare in the Lhasa block and no basaltic rocks have been found within the TYXR (e.g., Guo et al., 2013), suggesting that the intermediate ultrapotassic rocks are not be produced by fractional crystallization from basaltic magmas.

In summary, post-collisional ultrapotassic rocks of the TYXR have arc-like trace element patterns (enrichment in LREEs, LILEs, and Pb, but depletion in HFSEs) and very enriched crustal-like Sr-Nd-Pb isotope compositions. They have two groups of zircon O isotope compositions, corresponding to mantle and crust compositions, respectively. As noted above the geochemical compositions of these rocks are not significantly affected by low-temperature alteration, shallow-level crustal contamination, or fractional crystallization. Thus, these compositions are primarily inherited from a mantle source metasomatized by subducted crustal materials. In the following section we will use the B contents and $\delta^{11}B$ values to determine the nature of the crustal components recycled into the post-collisional mantle.

## 4.2 Origin of the light B isotope compositions

During mantle melting, Nb has similar bulk partition coefficients to B. However, during oceanic slab dehydration, B is strongly partitioned into aqueous fluids whereas Nb is retained in residual phases (e.g., rutile) in the subducted oceanic crust. These features make $\delta^{11}B$ and B/Nb values an ideal tracer of oceanic slab components. Slab-derived fluids preferentially mobilize B, especially $^{11}B$. As a result, subducted slab and slab-derived fluids will become progressively more depleted in B with lower $\delta^{11}B$ as dehydration progresses. Rosner et al., (2003) and others (see review in De Hoog and Savov, 2018) have shown that arc lavas further away from the trench have lower B/Nb ratios with lower $\delta^{11}B$ values. Another line of evidence comes from the high B concentration and $\delta^{11}B$ values of fore-arc serpentinites. Nearly all modern arc rocks plot between fore-arc serpentinite and MORB on a $\delta^{11}B$ vs B/Nb diagram (Fig. 8C) (see review in De Hoog and Savov, 2018). However, post-collisional ultrapotassic rocks from the TYXR show much lower B/Nb and $\delta^{11}B$ values than MORB, which indicates that they are unlikely to be generated by typical oceanic slab dehydration processes, unless the slab is extremely dehydrated. Chazi post-collisional ultrapotassic rocks from the TYXR are closer to the subduction zone than Rongniduo pre-collisional ultrapotassic rocks, yet, they have lower $\delta^{11}B$ than the latter (Fig. 8B). This is also inconsistent with a progressive dehydration model.

The Miocene ultrapotassic rocks in western Anatolia (Turkey) have very low $\delta^{11}$B (down to -31~ -20‰) (e.g., Palmer et al., 2019). Many studies have ascribed these very light B isotope compositions to the progressive dehydration of a stalled slab (e.g., Tonarini et al., 2005; Agostini et al., 2008; Sugden et al., 2020). In this model, the Oligocene-Miocene calc-alkaline rocks in western Anatolia exhibit B/Nb and $\delta^{11}$B values like those of modern arcs (Fig. 8C). Compared to these slightly older rocks, the Miocene K-rich rocks show a continuous decrease in $^{11}$B and B/Nb (Fig. 8C), and have $\delta^{11}$B lower than MORB. This has been interpreted to reflect fluid contribution from a stalled and extremely dehydrated slab with very low $\delta^{11}$B signatures and very low fluid-mobile element input to the sub-arc mantle. However, some TYXR samples have B/Nb ratios lower than those of MORB but similar to those of intra-plate and hot-arc lavas and Armenia post-collisional mafic rocks (Fig. 8C), both of which originated from a fluid-starved source. The Armenia post-collisional mafic rocks were derived from a mantle source metasomatized by melts of oceanic sediments (Sugden et al., 2020).

Oceanic sediment melts should be very common in sub-arc mantle during oceanic subduction, yet their low B/Nb and heavy B isotope signatures are easily obscured by a dominant aqueous fluid component in arc sources. However, the aqueous fluid component is transitory whereas the sediment melts have a much longer residence time in the mantle (Sugden et al., 2020). Once the oceanic slab detaches, the aqueous fluids are quickly removed, such that the B signature of sediment melts (i.e., heavy B isotopes and low B/Nb) could contribute to post-collisional (e.g., Armenia) mafic rocks after oceanic slab break-off (Fig. 8C). In the case of southern Tibet, the ~64 Ma ultrapotassic rocks from Rongniduo show arc-like and high B/Nb and $\delta^{11}$B like the western Anatolia calc-alkaline rocks, which is consistent with their derivation from an oceanic slab-modified mantle source (Fig. 8C). In comparison, the Miocene post-collisional rocks from the TYXR show much lower $\delta^{11}$B and B/Nb values. These compositions are clearly different from the scenario in Armenia (Fig. 8C) and cannot be ascribed to contributions of sediment melts. Based on all this evidence we conclude that the very light B isotope compositions of the TYXR post-collisional ultrapotassic rocks cannot be derived from a stalled oceanic slab or sediments alone.

Alternatively, the light B isotope compositions could be from partial melting of subducted continental crust. Palmer et al. (2019) suggested that the incorporation of B derived from deep-subducted continental crust may account for the low $\delta^{11}B$ observed in the western Anatolia K-rich volcanic rocks. They noted that phengite in the exhumed ultrahigh-pressure continental crustal rocks can show strongly negative $\delta^{11}B$ of -29‰. In the case of southern Tibet, the Tethyan Himalaya crust (including schist, gneiss, and Cenozoic S-type granitoids) shows very similar B contents and $\delta^{11}B$ values to post-collisional ultrapotassic rocks in the Lhasa block (Fig. 8A) (Fan et al., 2021). Thus, it is possible that the very light B isotope compositions of these post-collisional ultrapotassic rocks are sourced from recycled Indian upper continental crust. Subducted or delaminated lower crust should not primarily contribute to the formation of post-collisional ultrapotassic rocks due to their low $K_2O$ contents. Phengite is commonly present in subducted continental crust at ultrahigh-pressure conditions and can record very low $\delta^{11}B$ values. The breakdown of phengite would introduce not only the very light B isotope signatures but also highly potassic melts into the mantle source (Palmer et al., 2019), which can partially melt to form post-collisional ultrapotassic rocks in the Lhasa block.

## 4.3 Insights into the genesis of post-collisional ultrapotassic rocks

The post-collisional ultrapotassic rocks of the TYXR originate from an enriched mantle source that contains subducted slab components. Both subducted oceanic and continental crust can induce intensive crust-mantle interactions and yield the metasomatized lithospheric mantle, which can partially melt to produce post-collisional magmatism. In this study, B contents and $\delta^{11}B$ data have indicated that post-collisional ultrapotassic rocks in the Lhasa block could be derived from a mantle source enriched by subducted Indian upper continental crust. Mixing models show that the Sr-Nd isotope signatures of these rocks can be produced by mixing between ~8-40 wt.% crustal melts (e.g., partial melt of dehydrated Higher Himalayan Crystalline Sequence, Guo et al., 2013) and mantle endmembers (e.g., the depleted mantle, or a mixture of depleted mantle and enriched subcontinental lithospheric mantle) (Fig. 6). Large amounts of crustal melts in the mantle source can contribute to the distinct geochemical characteristics of these post-collisional rocks, e.g., andesitic and ultrapotassic compositions, enrichment in LILEs, Pb and LREEs, depletion in HFSEs and HREEs, and markedly enriched Sr-Nd-Pb-O isotopic signatures (Chen et al., 2021). In particular, high $K_2O$ contents (up to 11 wt.%, Fig. 4B) of the TYXR ultrapotassic rocks indicate that the highly potassic crustal melts were introduced into the mantle source by the breakdown of phengite during continental subduction (Soder and Romer, 2018).

The trace element signature of melts released from subducted continental crust was markedly affected by the stability of phases that sequester particular groups of elements. Numerous studies have noted that many ultrapotassic rocks are characterized by extremely high Th/La values (Tommasini et al., 2011; Wang et al., 2019), which distinguish them from subduction-related magmas worldwide (Fig. 9D). Given that lawsonite in blueschist with enriched continent-derived terrigenous origin can exhibit high Th/La values, Wang et al. (2019) suggested that blueschist-bearing mélange stored at shallow mantle depths can partially melt to generate high-Th/La post-collisional rocks. However, previous studies have demonstrated that post-collisional ultrapotassic rocks in the Lhasa block were likely derived from a garnet-facies mantle source (e.g., Hao et al., 2018). This is inconsistent with the lawsonite model which requires a shallow mantle source for post-collisional magmatism. Alternative repositories for Th and LREE in continental crust are monazite and allanite. However, these two minerals show contrasting fractionation behaviour of Th and La with $D_{Th/La}$ >1 for monazite and $D_{Th/La}$ <1 for allanite. Thus, partial melting of subducted continental crust with residual allanite may produce melts with high Th/La ratios (Soder and Romer, 2018). Melting with residual allanite should also produce elevated Sm/La ratios relative to upper continental crust. This is consistent with the observation that the majority of the TYXR ultrapotassic rocks show flat LREE systematics (i.e., high Sm/La) (Fig. 5A). Moreover, the samples show decreased Sm/La and Th/La ratios from south (Chazi) to north (Yaqian) (Fig. 9D), indicating decreasing amounts of restitic allanite. The Yaqian samples show fractionated LREEs (Fig. 5A), likely reflecting near-complete dissolution of allanite during continental crust subduction.

In summary, we suggest that the generation of post-collisional ultrapotassic rocks in southern Tibet can be explained by the interaction between the mantle and subducted Indian upper continental crust. Partial melting of deep-subducted Indian continental crust produces highly potassic felsic melts, which are enriched in LILEs and LREEs and have enriched Sr-Nd-Pb-O isotope compositions. These high-pressure silicate melts released from subducted continental crust are out of equilibrium with mantle wedge peridotite. Thus, extensive melt-peridotite interaction is likely to have occurred, consuming olivine to form mafic-ultramafic metasomatized mantle in a continental subduction channel (Dai et al., 2015). These metasomatites have a lower solidus compared to ambient peridotite and thus preferentially melt to form ultrapotassic magmas.

## 4.4 Tectonic implications

Previous studies have demonstrated that after Neo-Tethys oceanic slab break-off at ~45 Ma, the Himalaya-Tibet collision zone became a post-collisional intra-continental setting (e.g., Mo et al., 2008). However, the detailed post-collisional geodynamic processes remain uncertain. For example, models that invoke Lhasa lithospheric mantle thinning propose that Indian continental slab did not move further downward after oceanic slab break-off, due to its more buoyant nature relative to Asian lithosphere (e.g., Chung et al., 2005). Accordingly, the continuous northward impingement of India resulted in significant contraction of Lhasa lithospheric mantle (Chung et al., 2005). Subsequent lithospheric mantle thinning caused by the gravitational instability induced partial melting of the remaining lithospheric mantle to produce post-collisional ultrapotassic rocks. In this model, the mantle source of post-collisional magmatism is inherited from Lhasa lithospheric mantle, which was mostly metasomatized by protracted Neo-Tethys oceanic subduction with minor Indian continental subduction during the syn-collisional stage (Mahéo et al., 2009). However, the geochemical data presented above suggest that the mantle source of post-collisional ultrapotassic rocks was primarily metasomatized by subducted Indian continental crust rather than by oceanic subduction. Consequently, our study does not support the lithospheric thinning model.

Our preferred model is that Indian continental slab continued to subduct northward beneath the Lhasa block after Neo-Tethys oceanic slab break-off. In this model, given that continental subduction always proceeds at low thermal gradients and thus represents cold subduction, post-collisional magmatism in the Lhasa block could be considered as a result of Indian continental slab dynamics, e.g., slab tearing, roll-back, or break-off (Guo et al., 2013; DeCelles et al., 2011; Hao et al., 2019; Guo and Wilson, 2019). For example, Guo et al. (2013) suggested that the southward decreasing trend in the ages of post-collisional magmatism along the north-south-trending TangraYumco-Xuruco rift could support the Indian continental roll-back model. However, our zircon U-Pb ages indicate that these magmatic rocks erupted almost simultaneously. Our data when taken in conjunction with literature data (e.g., Hao et al., 2019; Guo and Wilson, 2019), lead us to propose a model of two-stage evolution (continental slab break-off followed by slab tearing) for the generation of post-collisional magmatism in the Lhasa block (Fig. 10).

Since ~25 Ma, significant north-south extension began to develop in southern Himalaya-Tibet orogen. This included the onset of the STDS (South Tibetan detachment system) and MCT (Main Central thrust) in the Himalaya block and the formation of the Kailas basin and Konglong A-type magmatism in the Lhasa block (see Hao et al., 2019 for details). This could indicate the break-off of subducted Indian continental plate, which also resulted in the east-west-trending magmatic belt. Geophysical data reveals two shallow anomalies beneath the India-Asia convergence zone, which have been attributed to detachment of northward-subducted Neo-Tethys oceanic lithosphere and Indian continental lithosphere (Replumaz et al., 2010).

The north-south extensional process ceased at ~18-17 Ma with a tectonic conversion to north-south contraction. This was marked by the development of the MBT (Main Boundary thrust), Main Frontier thrust, and widespread north-south-trending rifts in the Himalaya and Lhasa blocks (Williams et al., 2001). The north-south-trending ultrapotassic dikes and the post-collisional magmatism (e.g., TYXR rocks in this study) occurring within the north-south-trending rifts indicate significant east-west extension induced by deep mantle process (e.g., continental slab tearing). Continental slab tearing can contribute to an upwelling channel for the asthenosphere, which can produce magmatism and provide driving forces for the formation of the north-south-trending rifts. Geophysical data (e.g., seismic anisotropy) indicates that the geometry of subducted Indian continental slab beneath southern Tibet is characterized by systematic lateral variations, consistent with its tearing (e.g., Wu et al., 2019).

In summary, the B contents and $\delta^{11}B$ data of post-collisional ultrapotassic rocks in the Lhasa block indicate a mantle source metasomatized by deep-subducted Indian upper continental crust rather than by oceanic subduction. Combined with the spatial-temporal distribution of post-collisional magmatic rocks, tectonics and geophysical data, we propose that after Neo-Tethys oceanic slab break-off, Indian continental slab further northward subducted beneath southern Tibet and its subsequent break-off and tearing induced post-collisional magmatism in the Lhasa block of southern Tibet.

## 5. Conclusions

(1) Miocene (~13-11 Ma) post-collisional ultrapotassic volcanic rocks from the TangraYumco-Xuruco rift in the Lhasa block of southern Tibet are characterized by arc-type trace-element patterns, and very enriched Sr-Nd-Pb isotope compositions. They have two groups of zircon O isotopes, corresponding to the mantle and crustal compositions, respectively.

(2) These post-collisional rocks have significantly lower B/Nb and $\delta^{11}B$ values than oceanic subduction-related arcs (including pre-collisional (~64 Ma) ultrapotassic rocks in the Lhasa block in this study).

(3) The very light B isotope compositions of post-collisional ultrapotassic rocks in the Lhasa block originated from subducted Indian upper continental crust.

(4) Post-collisional magmatism in the Lhasa block was likely induced by the break-off and tearing of subducted Indian continental plate.

(5) Our study shows that melting of continental crust could generate post-collisional magmas with high Th/La ratios, enriched Sr-Nd-Pb isotopes and very light B isotope signatures. These characteristics could be used to distinguish these lavas from

ultrapotassic lavas in oceanic subduction settings.

## Acknowledgements

We are very grateful to the editor Professor Rosemary Hickey-Vargas and two anonymous reviewers for their detailed and constructive comments which greatly improved the manuscript. Financial support for this research was provided by the Second Tibetan Plateau Scientific Expedition and Research (STEP) (2019QZKK0702), and the National Natural Science Foundation of China (42021002, 91855215, 42073025), the Youth Innovation Promotion Association CAS (2022357), and the Strategic Priority Research Program (A) of the Chinese Academy of Sciences (grant no. XDA2007030402). This is contribution No. XXX from GIGCAS.

## References

Agostini, S., Ryan, J.G., Tonarini, S., Innocenti, F., 2008. Drying and dying of a sub-ducted slab: coupled Li and B isotope variations in western Anatolia Cenozoic volcanism. Earth and Planetary Science Letters, 272, 139-147.

Azizi, H., Daneshvar, N., Mohammadi, A., Asahara, Y., Whattam, S., Tsuboi, M., Minami, M., 2021, Early Miocene post-collision andesite in the Takab area, northwest Iran, Journal of Petrology, 62, 7, egab022.

Chen, L., Zheng, Y-F., Xu, Z., Zhao, Z.-F., 2021. Generation of andesite through partial melting of basaltic metasomatites in the mantle wedge: Insight from quantitative study of Andean andesites. Geoscience Frontiers, 12, 101124.

Chung, S.L., Chu, M.-F., Zhang, Y., Xie, Y., Lo, C.-H., Lee, T.-Y., Lan, C.-Y., Li, X-H., Zhang, Q., Wang, Y., 2005. Tibetan tectonic evolution inferred from spatial and temporal variations in post-collisional magmatism. Earth-Science Reviews, 68(3-4), 173-196.

Conticelli, S., Guarnieri, L., Farinelli, A., Mattei, M., Avanzinelli, R., Bianchini, G., Boari, E., Tommasini, S., Tiepolo, M., Prelevic, D., Venturelli, G., 2009. Trace elements and Sr-Nd-Pb isotopes of K-rich to shoshonitic, and calc-alkalic magmatism of the Western Mediterranean region: genesis of ultrapotassic to calc-alkaline magmatic associations in a post-collisional geodynamic setting. Lithos, 107, 68-92.

Dai, L.-Q., Zhao, Z.-F., Zheng, Y.-F., 2015. Tectonic development from oceanic subduction to continental collision: Geochemical evidence from postcollisional mafic rocks in the Hong'an-Dabie orogens. Gondwana Res. 27, 1236-1254.

Davidson, J., Turner, S., Handley, H., Macpherson, C., Dosseto, A., 2007. Amphibole “sponge” in arc crust? Geology, 35, 787-790.

De Hoog, J.C.M., Savov, I.P., 2017, Boron isotopes as a tracer of subduction zone processes, in Marschall, H.R., and Foster, G.L., eds., Boron Isotopes: The Fifth Element: Cham, Switzerland, Springer

Nature, p. 217-247.

DeCelles, P.G., Kapp, P., Quade, J., Gehrels, G.E., 2011, Oligocene-Miocene Kailas basin, southwestern Tibet: Record of postcollisional upper-plate extension in the Indus-Yarlung suture zone: Geological Society of America Bulletin, 123, 1337-1362.

Ding, L., Kapp, P., Zhong, D. L., Deng, W. M., 2003. Cenozoic volcanism in Tibet: Evidence for a transition from oceanic to continental subduction. Journal of Petrology, 44(10), 1833-1865.

Ducea, M, 2016. RESEARCH FOCUS: Understanding continental subduction: A work in progress. Geology, 44(3), 239-240.

Elliott, T., 2004, Tracers of the slab: Geophysical Monograph, 138, 23-45.

Fan, J-J., Wang, Q., Li, J., Wei, G-J., Ma, J-L., Ma, L., Li, Q-W., Jiang, Z-Q., Zhang, L., Wang, Z-L., Zhang, L., 2021, Boron and molybdenum isotopic fractionation during crustal anatexis: Constraints from the Conadong leucogranites in the Himalayan Block, South Tibet: Geochimica et Cosmochimica Acta 297, 120-142.

Foster, G.L., Pogge von Strandmann, P.A.E., Rae, J.W.B., 2010. Boron and magnesium isotopic composition of seawater. Geochemistry Geophysics Geosystems, 11, Q08015.

Gao, Y.F., Hou, Z.Q., Kamber, B.S., Wei, R.H., Meng, X.J., 2007. Lamproitic rocks from continental collision zones: evidence for recycling of subducted Tethyan oceanic sediments in southern Tibet. Journal of Petrology, 48, 729-752.

Gómez-Tuena, A., Cavazos-Tovar, J.G., Parolari, M., Straub, S.M., Espinasa-Pereña, R., 2018. Geochronological and geochemical evidence of continental crust ‘relamination’ in the origin of intermediate arc magmas. Lithos, 322, 52-66.

Guo, Z.F., Wilson, M., 2019. Late Oligocene-early Miocene transformation of postcollisional magmatism in Tibet: Geology, 47, 776-780.

Guo, Z.F., Wilson, M., Zhang, M.L., Cheng, Z.H., Zhang, L.H., 2013. Post-collisional, K-rich mafic magmatism in south Tibet: constraints on Indian slab-to-wedge transport processes and plateau uplift. Contributions to Mineralogy and Petrology, 165, 1311-1340.

Hao, L.-L., Wang, Q., Wyman, D.A., Ma, L., Xia, X.P., Ou, Q., 2019. First identification of postcollisional A-type magmatism in the Himalayan-Tibetan orogen: Geology, 47, 187-190.

Hao, L.L., Wang, Q., Wyman, D.A., Qi, Y., Ma, L., Huang, F., Zhang, L., Xia, X.P., Ou, Q., 2018, First identification of mafic igneous enclaves in Miocene lavas of southern Tibet with implications for Indian continental subduction: Geophysical Research Letters, 45, 8205-8213.

Hu, X., Garzanti, E., Moore, T., Raffi, I., 2015. Direct stratigraphic dating of India-Asia collision onset at the Selandian (middle Paleocene, 59±1 Ma). Geology, 43(10), 859-862.

Leeman, W.P., Tonarini, S., Chan, L.H., Borg, L.E., 2004. Boron and lithium isotopic variations in a hot subduction zone -the southern Washington Cascades. Chem Geol. 212, 101-124.

Liu, D., Zhao, Z., Zhu, D., Niu, Y., Widom, E., Teng, F., DePaolo, D.J., Ke, S., Xu, J-F., Wang, Q., Mo, X-X., 2015. Identifying mantle carbonatite metasomatism through Os-Sr-Mg isotopes in Tibetan ultrapotassic rocks. Earth and Planetary Science Letters, 458-469.

Mahéo, G., Blichert-Toft, J., Pin, C., Guillot, S., Pecher, A., 2009, Partial melting of mantle and crustal sources beneath south Karakorum, Pakistan: Implications for the Miocene geodynamic evolution of the India-Asia Convergence Zone. Journal of Petrology, 50, 3, 427-449.

Marschall, H.R., Wanless, V.D., Shimizu, N., Pogge von Strandmann, P.A.E., Elliott, T., Monteleone, B.D., 2017. The boron and lithium isotopic composition of mid-ocean ridge basalts and the mantle. Geochim. Cosmochim. Acta 207, 102-138.

Mo, X., Niu, Y., Dong, G., Zhao, Z., Hou, Z., Zhou, S., Ke, S., 2008. Contribution of syncollisional felsic magmatism to continental crust growth: A case study of the Paleogene Linzizong volcanic succession in southern Tibet. Chemical Geology, 250, 49-67.

Palmer, M.R., Ersoy, E.Y., Akal, C., Uysal, İ., Genç, Ş.C., Banks, L.A., Cooper, M.J., Milton, J.A., Zhao, K.D., 2019, A short, sharp pulse of potassium-rich volcanism during continental collision and subduction: Geology, 47, 1079-1082.

Qi, Y., Gou, G. N., Wang, Q., Wyman, D. A., Jiang, Z. Q., Li, Q. L., Zhang, L., 2018. Cenozoic mantle composition evolution of southern Tibet indicated by Paleocene (~64 Ma) pseudoleucite phonolitic rocks in Central Lhasa Terrane. Lithos, 302-303, 178-188.

Replumaz, A., Negredo, A.M., Villaseñor, A., Guillot, S., 2010, Indian continental subduction and slab break-off during Tertiary collision: Terra Nova, 22, 290-296.

Rosner, M., Erzinger, J., Franz, G., Trumbull, R.B., 2003, Slab-derived boron isotope signatures in arc volcanic rocks from the Central Andes and evidence for boron isotope fractionation during progressive slab dehydration. Geochemistry Geophysics Geosystems, 4, 9005.

Rudnick, R.L. Gao, S., 2003. Composition of the continental crust: Treatise on Geochemistry, 3, 659.

Soder, C., Romer, R., 2018, Post-collisional Potassic-Ultrapotassic Magmatism of the Variscan Orogen: Implications for Mantle Metasomatism during Continental Subduction: Journal of Petrology, 59, 6, 1007-1034.

Stern, R.J., 2002, Subduction zones: Reviews of Geophysics, 40, 4, 3-1-3-38.

Sugden, P., Savova, I., Agostini, S., Wilson, M., Halama, F., Meliksetian, K., 2020, Boron isotope insights into the origin of subduction signatures in continent-continent collision zone volcanism. Earth and Planetary Science Letters, 538, 116207.

Tang, M., Rudnick, R., Chauvel, C., 2014, Sedimentary input to the source of Lesser Antilles lavas: A Li perspective: Geochimica Et Cosmochimica Acta, 144, 43-58.

Tian, S.-H., Hou, Z., Mo, X., Tian, Y., Zhao, Y., Hou, K., Yang, Z., Hu, W., Li, X., Zhang, Y., 2020, Lithium isotopic evidence for subduction of the Indian lower crust beneath southern Tibet: Gondwana Research, 77, 168-183.

Tian, S-H., Yang, Z-S., Hou, Z-Q., Mo, X-X., Hu, W-J., Zhao, Y., Zhao, X-Y., 2017, Subduction of the Indian lower crust beneath southern Tibet revealed by the post-collisional potassic and ultrapotassic rocks in SW Tibet. Gondwana Research, 41, 29-50

Tommasini, S., Avanzinelli, R., Conticelli, S., 2011. The Th/La and Sm/La conundrum of the Tethyan realm lamproites. Earth and Planetary Science Letters, 301(3-4), 469-478.

Tonarini, S., Agostini, S., Innocenti, F., Manetti, P., 2005. δ11B as tracer of slab dehydration and mantle evolution in western Anatolia Cenozoic magmatism. Terra Nova 17, 259-264.

Tonarini, S., Leeman, W.P., Leat, P.T., 2011. Subduction erosion of forearc mantle wedge implicated in the genesis of the South Sandwich Island (SSI) arc: evidence from boron isotope systematics. Earth and Planetary Science Letters, 301(1-2): 275-284

Trumbull, R.B., Slack, J.F., 2018. Boron isotopes in the continental crust: Granites, pegmatites, felsic volcanic rocks, and related ore deposits. In: Trumbull, Robert B., Slack, John F. (Eds.), Boron Isotopes-The Fifth Element. Advances in Isotope Geochemistry. Springer, Cham, pp. 249-272.

Vannucchi, P., Galeotti, S., Clift, P.D., Ranero, C.R., von Huene, R., 2004. Long-term subduction-erosion along the Guatemalan margin of the middle America trench. Geology, 32, 617-620.

Wang, Y., Prelević, D., Foley. S., 2019. Geochemical characteristics of lawsonite blueschists in tectonic mélange from the Tavşanlı Zone, Turkey: Potential constraints on the origin of Mediterranean

potassium-rich magmatism. American Mineralogist, 104(5), 724-743.
Willbold, M., Stracke, A., 2010. Formation of enriched mantle components by recycling of upper and lower continental crust. Chemical Geology, 276(3), 188-197.
Williams, H., Turner, S., Kelley, S., Harris, N., 2001. Age and composition of dikes in southern Tibet: New constraints on the timing of east-west extension and its relationship to postcollisional volcanism: Geology, 29, 339-342.
Wu, C., Tian, X., Xu, T., Liang, X., Chen, Y., Taylor, M., Badal, J., Bai, Z., Duan, Y., Yu, G., Teng, J., 2019. Deformation of crust and upper mantle in central Tibet caused by the northward subduction and slab tearing of the Indian lithosphere: new evidence based on shear wave splitting measurements. Earth and Planetary Science Letters, 514, 75-83.
Yakovlev, P., Saal, A., Clark, M., Hong, C., Niemi, A., Mallick, S., 2019, The geochemistry of Tibetan lavas: Spatial and temporal relationships, tectonic links and geodynamic implications. Earth and Planetary Science Letters, 520, 115-126.
Yin, A., Harrison, T.M., 2000, Geologic evolution of the Himalayan-Tibetan orogen: Annual Review of Earth and Planetary Sciences, 28, 211-280.
Zheng, Y.-F., Chen, Y.-X., 2016. Continental versus oceanic subduction zones. Natl. Sci. Rev. 3, 495-519.
Zhu, D.-C., Zhao, Z.-D., Niu, Y.-L., Mo, X.-X., Chung, S.-L., Hou, Z.-Q., Wang, L.-Q., Wu, F.-Y., 2011. The Lhasa terrane: record of a microcontinent and its histories of drift and growth. Earth and Planetary Science Letters, 301, 241-255.

# Figure captions

**Fig. 1** (A) Overview map showing the distribution of Cenozoic magmatic rocks in the Lhasa block of southern Tibet, after Guo et al. (2013). 1, post-collisional K-rich magmatic rocks; 2, post-collisional adakitic rocks; 3, Linzizong volcanic successions; 4, Rongniduo pre-collisional (~64 Ma) ultrapotassic rocks (Qi et al., 2018). The blue rectangle shows the location of the study area (TangraYumco-Xuruco rift). The dashed lines show the main tectonic sutures. JS= Jinsha suture, BN= Bangong-Nujiang suture, IYZ= Indus-Yarlung-Zangbu suture, MBT= Main Boundary Thrust. (B) Map showing the distribution of post-collisional K-rich magmatic rocks within the TangraYumco-Xuruco rift (modified from Guo et al., 2013). The numbers in circles represent the individual volcanic fields as follows: 1, Yaqian; 2, Mibale; 3, Daguo; 4, Chazi. The age data are shown in detail in the text.

**Fig. 2** Representative photomicrographs of the TangraYumco-Xuruco ultrapotassic rocks. A-D: samples from Yaqian, Mibale, Daguo and Chazi, respectively. Ol= olivine; Cpx= clinopyroxene; Phl= phlogopite; Kfs= K-feldspar.

**Fig. 3** Zircon U-Pb age and O isotope plots for the Chazi ultrapotassic rocks from the TangraYumco-Xuruco rift. (A) weighted mean age plot. (B) zircon O isotope analyses from samples CZ02-4, 07-1, and 08-1.

**Fig. 4** The TangraYumco-Xuruco ultrapotassic rocks plotted on (A) total alkalis versus silica and (B) potassium vs. sodium. The Rongniduo samples (Qi et al., 2018) are shown for comparison.

**Fig. 5** (A) Chondrite-normalized REE patterns and (B) primitive mantle-normalized trace element distribution patterns for the TangraYumco-Xuruco ultrapotassic rocks. The data for Rongniduo samples are from Qi et al. (2018).

**Fig. 6** Sr-Nd isotope plot for post-collisional (13-11 Ma) ultrapotassic rocks in the TangraYumco-Xuruco rift in the Lhasa block. Pre-collisional (64 Ma) ultrapotassic rocks from Rongniduo in the Lhasa block are also shown for comparison (Qi et al., 2018). The mixing endmembers DMM (depleted MORB mantle) and partial melt of dehydrated HHCS (Higher Himalayan Crystalline Sequence) are from Guo et al. (2013) and references therein. The DMM+E-SCLM (enriched subcontinental lithospheric mantle) is from Chen et al. (2021). The data for post-collisional ultrapotassic rocks elsewhere in the Lhasa block are from Hao et al. (2018) and references therein.

**Fig. 7** Pb isotope plot for the TYXR ultrapotassic rocks. Lead evolution curves for mantle (M), orogen (O) and upper crust (UC) are from Soder and Romer (2018) and references therein.

**Fig. 8** (A) boron contents, (B) sampling latitudes, and (C) B/Nb ratios versus $\delta^{11}B$ (‰) for post-collisional (13-11 Ma) ultrapotassic rocks in the TangraYumco-Xuruco rift (TYXR). Pre-collisional (64 Ma) Rongniduo ultrapotassic rocks are also shown for comparison. The B contents and $\delta^{11}B$ values of the Tethyan Himalaya crust are from Fan et al. (2021). The data for the western Anatolia calc-alkaline (CA), ultrapotassic (UK), and intra-plate alkaline (Alk) rocks are from Tonarini et al. (2005) and Agostini et al. (2008). The data for post-collisional mafic rocks in Armenia are from Sugden et al. (2020). The data for a hot arc (Cascades) are from Leeman et al. (2004). The data for arc rocks with typical oceanic slab dehydration are from De Hoog and Savov (2017). The B/Nb (0.15-1.05) and $\delta^{11}B$ ($-7.1\pm 0.9$‰) values of MORB are from Marschall et al. (2017).

**Fig. 9** (A) La/Yb vs Mg#; (B-C) La vs La/Yb and La/Sm, respectively. The TYXR post-collisional rocks fall along the trend of partial melting (PM) rather than fractional crystallization (FC). (D) Th/La vs. Sm/La. Note the distinction between ultrapotassic rocks (including the Tethyan realm lamproites, Tommasini et al., 2011) and normal arc magmas (Wang et al., 2019 and references therein). The average upper continental crust (UC) is from Rudnick and Gao (2003). The vectors of residual allanite and monazite are after Soder and Romer (2018).

**Fig. 10** Cartoon diagrams showing post-collisional tectono-magmatic model in the Lhasa block of southern Tibet, modified from Guo and Wilson (2019) and Hao et al. (2019). (A) Indian continental slab breakoff during 25-18 Ma. This process resulted in significant north-south extension in southern Himalaya-Tibet orogen (see Hao et al., 2019 for details). (B) Indian continental slab tearing during 18-8 Ma. The north-south extensional process ceased at ~18-17 Ma with a tectonic conversion to north-south contraction. After ~8 Ma, Indian continental slab began to subduct northward beneath the Lhasa block, coinciding with a lack of magmatism from 8 Ma to present. IYZS, Indus-Yarlung-Zangbu suture; BNS, Bangong-Nujiang suture; JS, Jinsha suture; KS, Kunlun suture.

Figure 1

Click here to access/download;Figure;Fig-1.pdf

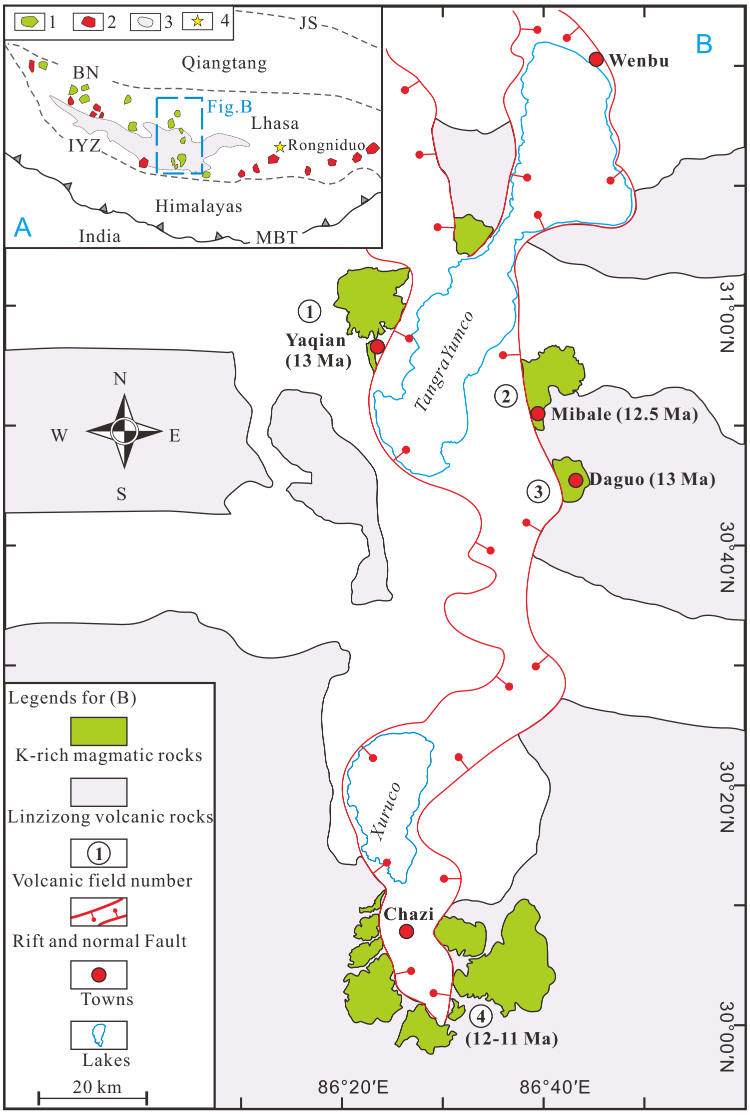

Figure 2



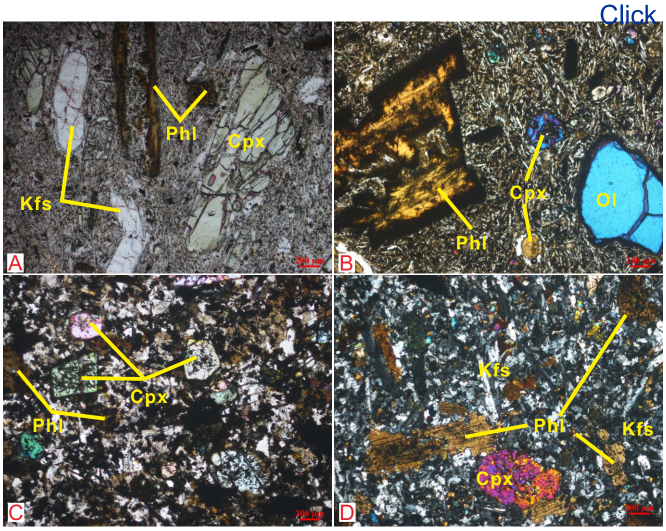

Figure 3



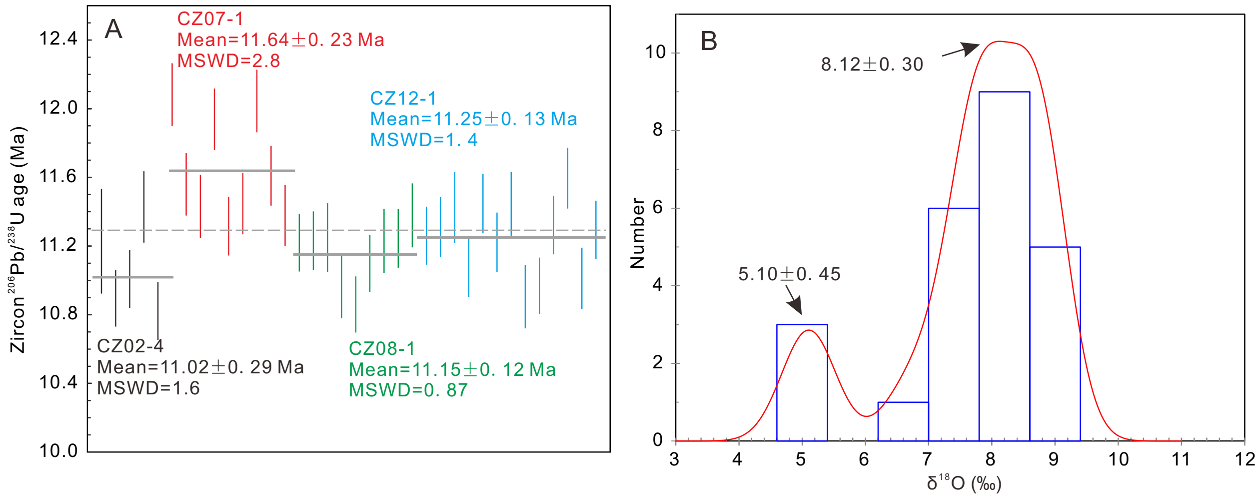

A
CZ07-1
Mean=11.64±0. 23 Ma
MSWD=2.8
CZ12-1
Mean=11.25±0. 13 Ma
MSWD=1. 4
CZ02-4
Mean=11.02±0. 29 Ma
MSWD=1.6
CZ08-1
Mean=11.15±0. 12 Ma
MSWD=0. 87
Zircon $^{206}Pb/^{238}U$ age (Ma)
12.4
12.0
11.6
11.2
10.8
10.4
10.0
B
8.12±0. 30
5.10±0. 45
Number
10
8
6
4
2
0
3
4
5
6
7
8
9
10
11
12
$\delta^{18}O$ (‰)

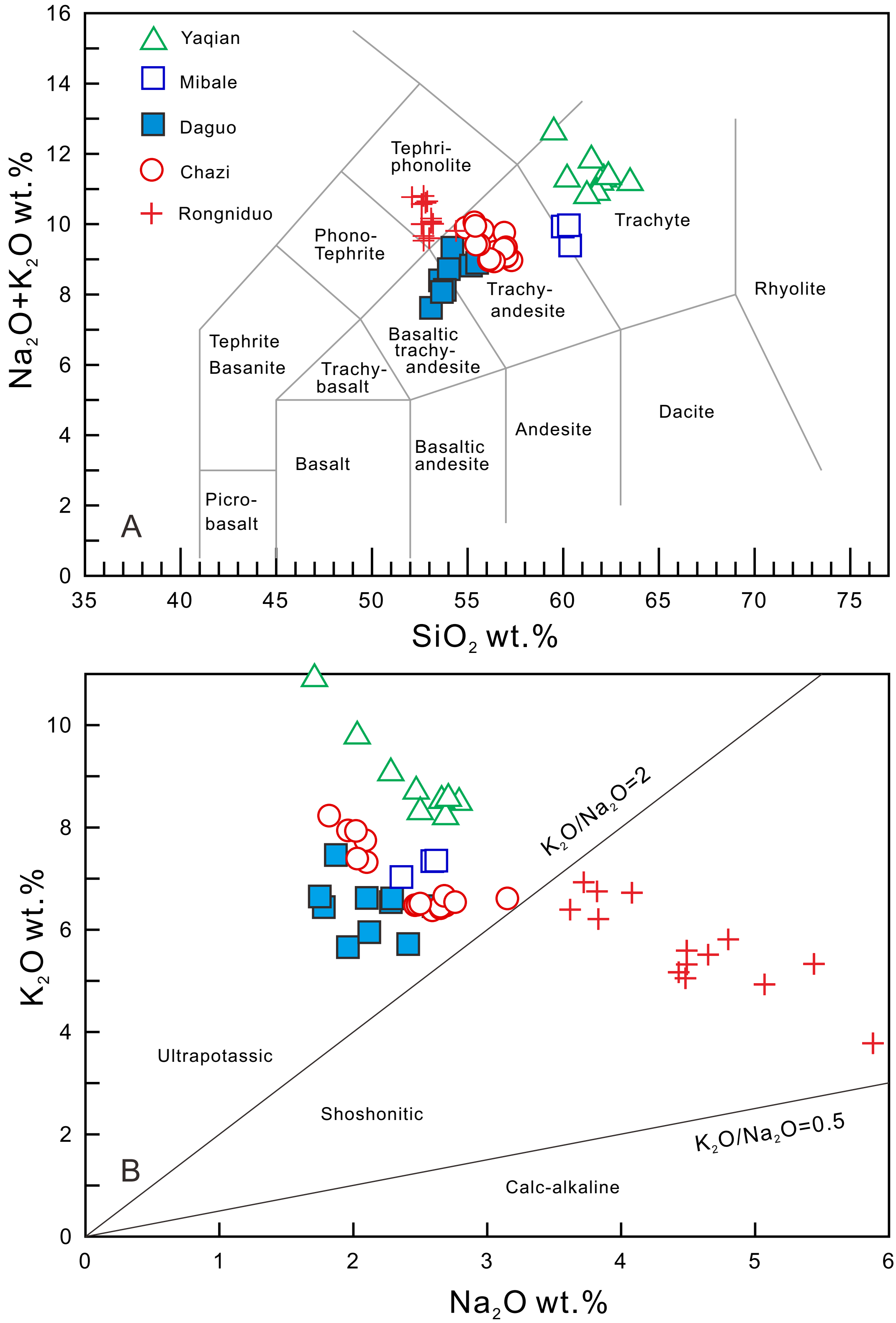
Yaqian
Mibale
Daguo
Chazi
Rongniduo
Tephri-
phonolite
Phono-
Tephrite
Trachyte
Rhyolite
Trachy-
andesite
Basaltic
trachy-
andesite
Tephrite
Basanite
Trachy-
basalt
Andesite
Dacite
Basaltic
andesite
Basalt
Picro-
basalt
A
$Na_2O+K_2O$ wt.%
$SiO_2$ wt.%
$K_2O/Na_2O=2$
Ultrapotassic
Shoshonitic
$K_2O/Na_2O=0.5$
Calc-alkaline
B
$K_2O$ wt.%
$Na_2O$ wt.%

Figure 5

Click here to access/download;Figure;Fig-5.pdf

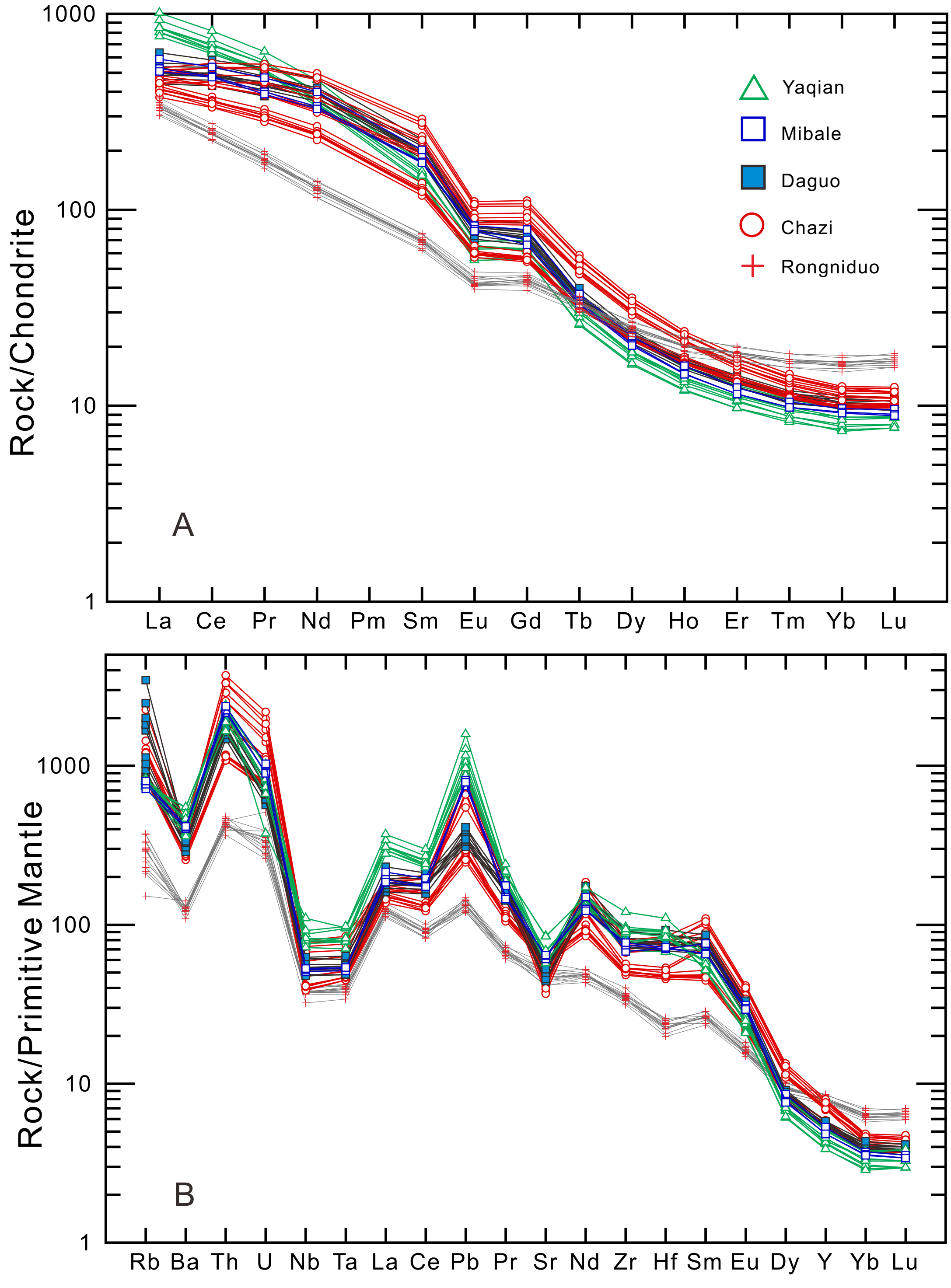

 

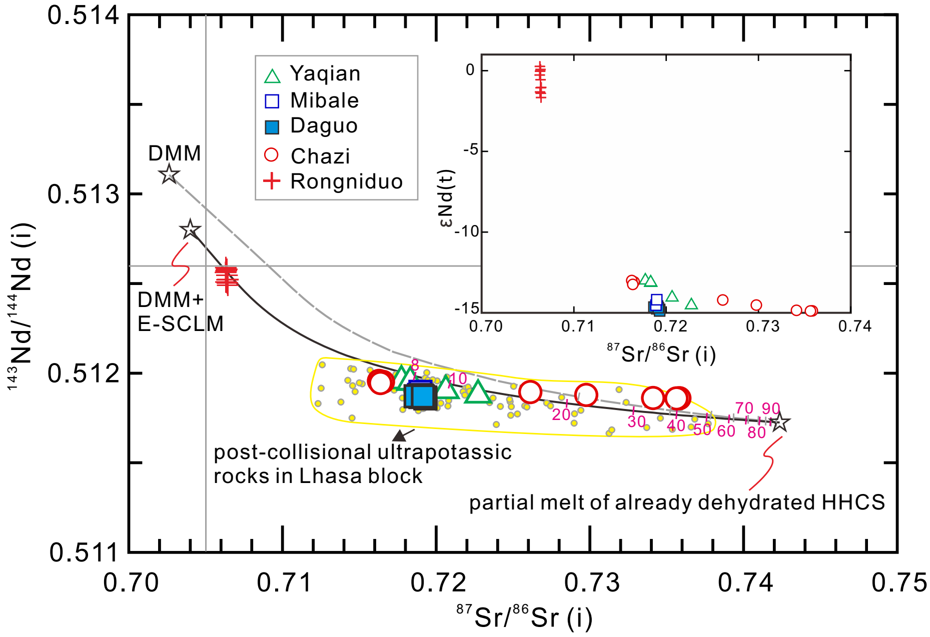

0.514
0.513
0.512
0.511
0.70
0.71
0.72
0.73
0.74
0.75
$^{143}Nd/^{144}Nd$ (i)
$^{87}Sr/^{86}Sr$ (i)
Yaqian
Mibale
Daguo
Chazi
Rongniduo
DMM
DMM+
E-SCLM
post-collisional ultrapotassic
rocks in Lhasa block
partial melt of already dehydrated HHCS
εNd(t)

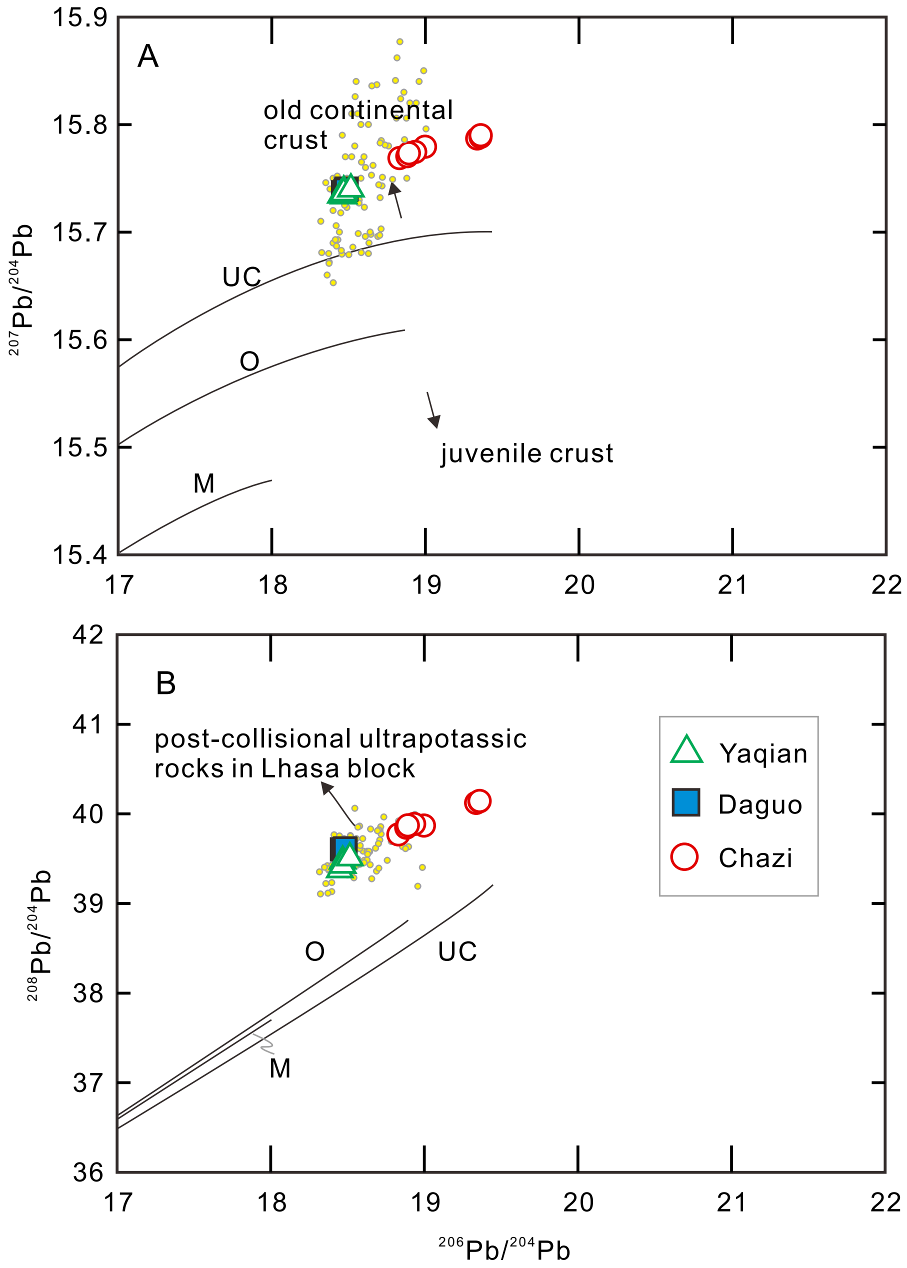

15.9
A
old continental
crust
15.8
15.7
UC
O
15.6
15.5
juvenile crust
M
15.4
17
18
19
20
21
22
$^{207}Pb/^{204}Pb$
42
B
41
post-collisional ultrapotassic
rocks in Lhasa block
40
39
O
UC
38
37
M
36
Yaqian
Daguo
Chazi
$^{208}Pb/^{204}Pb$
$^{206}Pb/^{204}Pb$

Figure 8

Click here to access/download;Figure;Fig-8.pdf

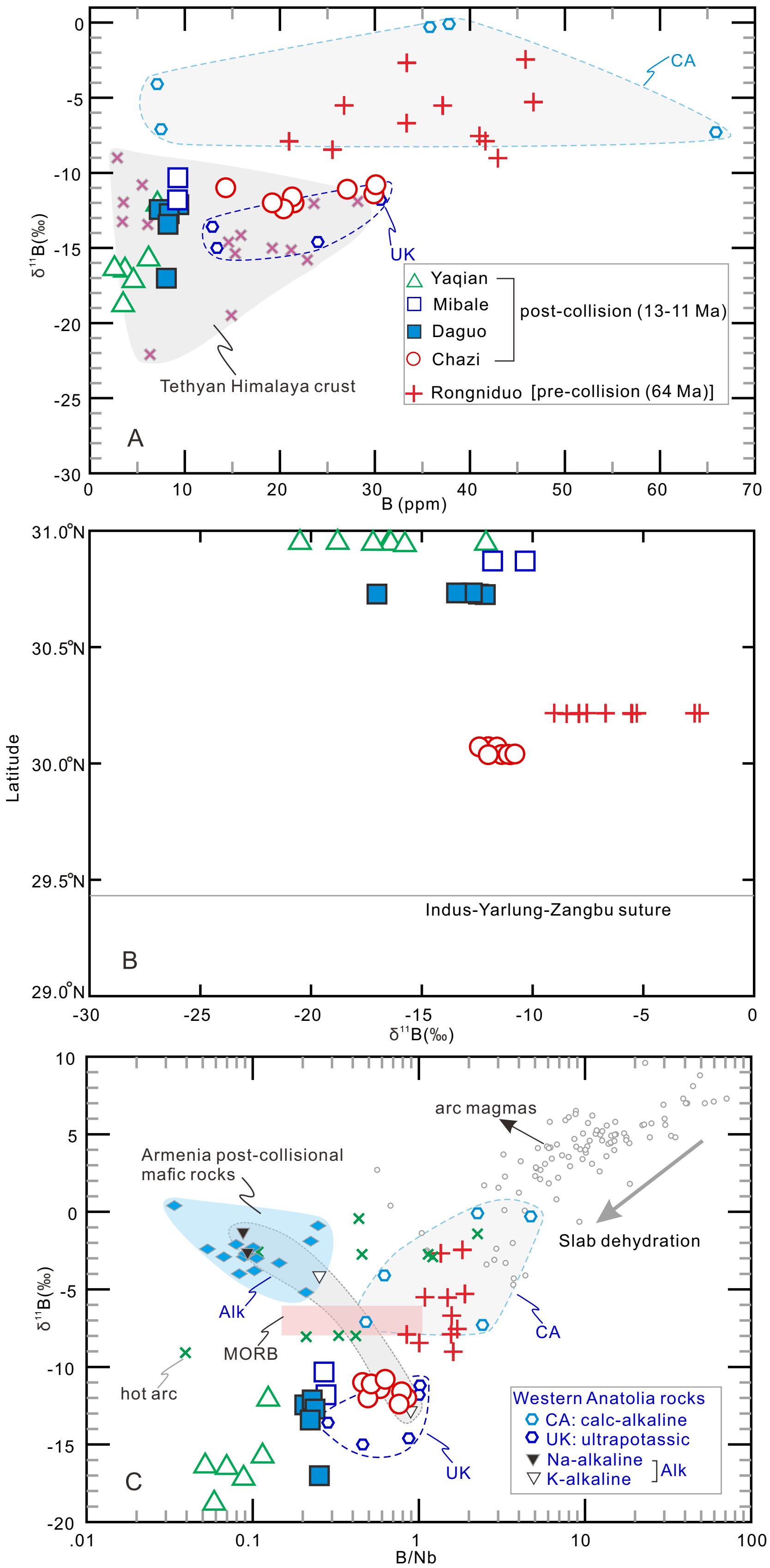

Figure 9



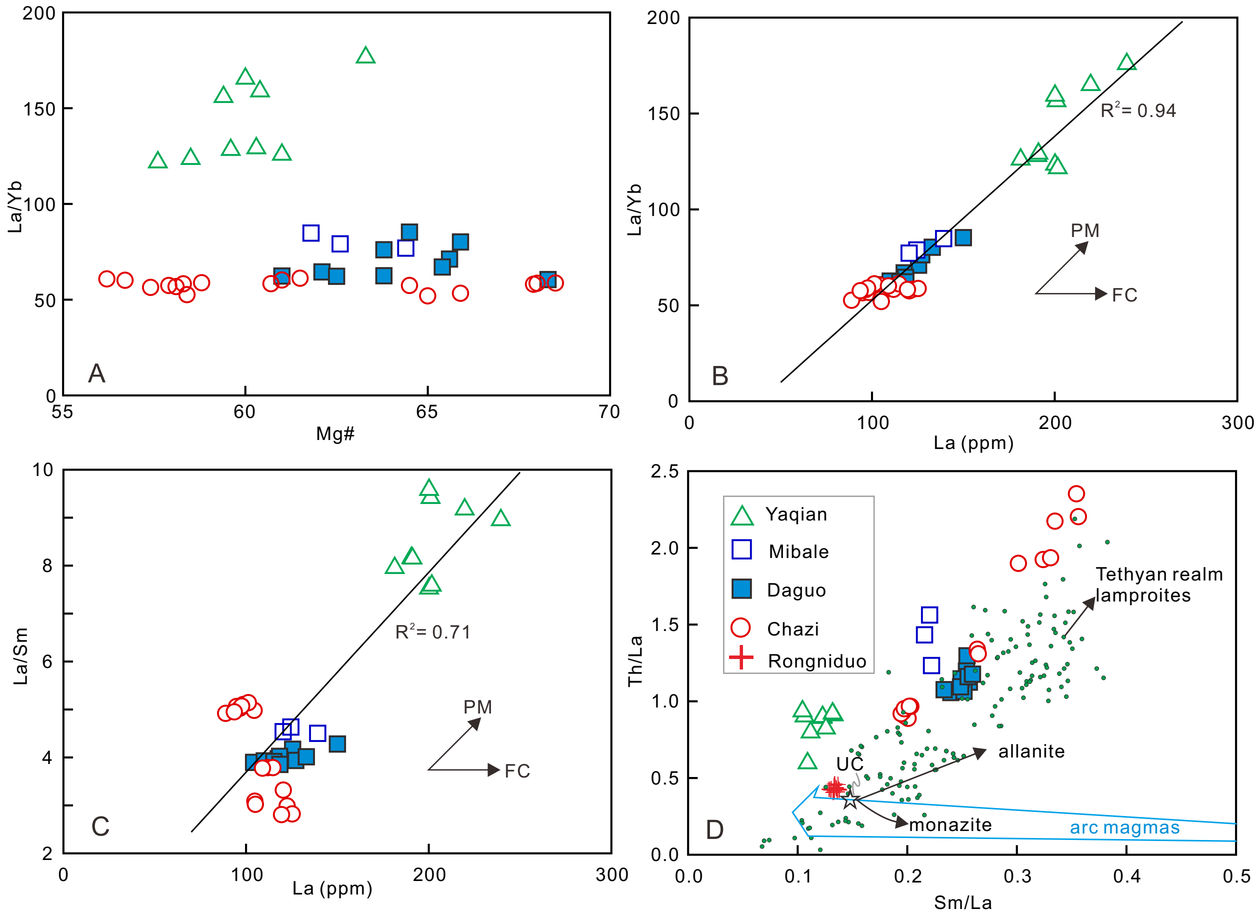
A
La/Yb
Mg#
B
La/Yb
La (ppm)
$R^2$= 0.94
PM
FC
C
La/Sm
La (ppm)
$R^2$= 0.71
PM
FC
D
Th/La
Sm/La
Yaqian
Mibale
Daguo
Chazi
Rongniduo
Tethyan realm lamproites
allanite
monazite
UC
arc magmas

Figure 10

Click here to access/download;Figure;Fig-10.pdf

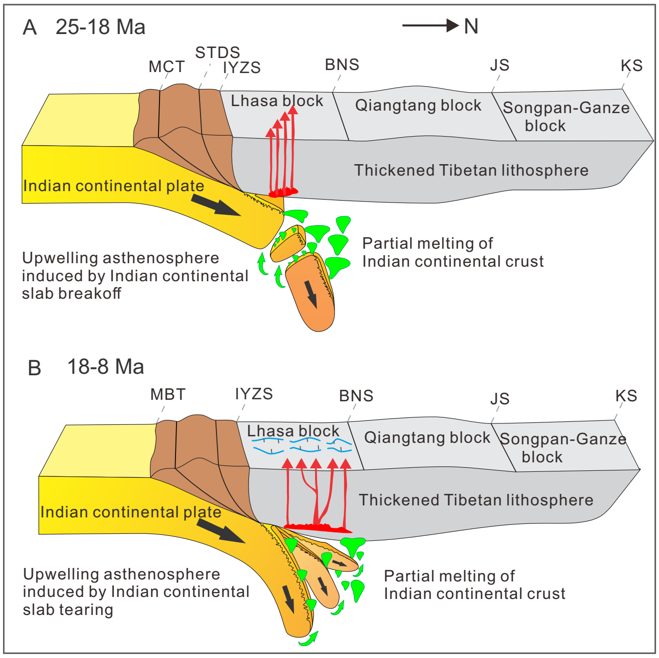

Click here to access/download

**Supplementary material for online publication only**

Appendix.pdf

## Credit author statement

**Lu-Lu Hao:** Conceptualization, Methodology, Formal analysis, Investigation, Writing – original draft, Writing – review & editing. **Qiang Wang**: Conceptualization, Methodology, Investigation, Formal analysis, Writing – original draft, Writing – review & editing. **Andrew C. Kerr**: Formal analysis, Writing – original draft, Writing – review & editing. **Gang-Jian Wei**: Methodology, Formal analysis, Investigation, Writing – review & editing. **Fang Huang**: Formal analysis, Writing – review & editing. **Miao-Yan Zhang**: Methodology, Formal analysis, Writing – review & editing. **Yue Qi:** Investigation, Writing – review & editing. **Lin Ma:** Investigation, Writing – review & editing. **Xue-Fei Chen:** Methodology, Formal analysis, Writing – review & editing. **Ya-Nan Yang:** Methodology, Formal analysis, Writing – review & editing.

## Declaration of interests

The authors declare that they have no known competing financial interests or personal relationships that could have appeared to influence the work reported in this paper.